Materials and Structures (2026) 59:315
https://doi.org/10.1617/s11527-026-03191-5

ORIGINAL ARTICLE

Mechanical and microstructural properties of user-friendly one-part alkali-activated mortars via low-grade calcined clay

Oğuzhan Öztürk · Jitong Zhao · Cesare Signorini · Thomas Köberle · Marco Liebscher · Viktor Mechtcherine

Received: 27 February 2026 / Revised: 25 May 2026 / Accepted: 6 July 2026

Abstract Alkali-activated materials (AAMs) have emerged as a promising alternative to traditional cement-based binders. However, their adoption is restricted by non-user-friendly production processes, the need for curing at elevated temperatures when higher amounts of aluminosilicate sources are used and the limited availability or regional dependency of precursors and activators. This study focuses on the development of one-part AAMs made with low-kaolinitic calcined clays as the main precursor (between 63–100%wt.) cured at ambient temperature. A comprehensive assessment of reaction kinetics, rheology and mechanical/microstructural properties was conducted. Results demonstrate promising fresh and hardened properties with an optimal AAM formulation including 81% of calcined clay achieving a flow diameter of 17 cm, initial/final setting times ranging from 50 to 116 minutes and 28-day compressive strength of approximately 40 MPa. Low-volume slag governs hydration kinetics and microstructure by supplying calcium-rich species and nucleation sites that activate ambient-temperature reactions and promote hybrid gel formation. It modulates setting time and refine porosity toward meso scales. Alongside an optimized solid-silicate regime, this slag-limited formulation optimizes ambient-cured fresh and hardened properties yielding a site-ready binder for multi-purpose applications. The study represents an attractive opportunity for a broader use of low-grade calcined clays as a practical and sustainable alternative to Portland-cement-based binders.

Keywords Alkali activated materials · Calcined clays · One-part AAM · Hydration · Microstructure

1 Introduction

Due to the increasing urbanization in developing countries, the global demand for Portland cement (PC) is expected to grow steadily in the coming decades, raising serious sustainability concerns in the construction industry and forcing the scientific community to rethink traditional binders [1–4]. Among the cement-free alternatives, alkali-activated materials (AAMs) have been extensively studied in recent decades [5–8] and are considered as a promising substitute for PC [9–12]. However, factors such as changes in availability of raw materials, regional reliance, and the corresponding challenge

O. Öztürk
Civil Engineering Department, Konya Technical University, 42250 Konya, Turkey

J. Zhao · C. Signorini (✉) · T. Köberle · M. Liebscher · V. Mechtcherine
Institute of Construction Materials, TU Dresden, 01062 Dresden, Germany
e-mail: cesare.signorini@tu-dresden.de

C. Signorini · T. Köberle · M. Liebscher · V. Mechtcherine
Cluster of Excellence CARE, TU Dresden and RWTH Aachen, Dresden / Aachen, Germany

Published online: 19 July 2026

of long-distance transportation, represent an obstacle for the large-scale production required to meet the global demand. Furthermore, key precursors such as fly ash, slag and metakaolin are already widely and efficiently employed as supplementary cementitious materials (SCMs) in blended binders, rather than being prioritized for AAMs [12]. On the other hand, other industries, such as paper or ceramics, require significant amounts of high-purity kaolinite, which is scarcely available worldwide, although it currently represents the main source of metakaolin, which is one of the most studied precursors for low-calcium AAMs, i.e., geopolymers [13]. This underscores the urgent need to diversify the spectrum of aluminosilicate sources [14], integrating technical, scalability and sustainability criteria. Besides their use in blended cementitious binders [15], low-grade calcined clays have recently attracted attention with the aim of expanding the production capabilities of AAMs [14, 16], while addressing the environmental impacts associated with existing AAM precursors. In addition, the use of globally abundant clay minerals holds promise as a research avenue for the widespread adoption of an emerging family of AAMs, i.e. the so-called "one-part" AAMs. Indeed, conventional AAMs are produced through a reaction between liquid alkali solutions and solid precursors [17–20]. Most of the studies focused on alkali activators with Si_2O/Na_2O molar ratios below 1.25, which are often considered corrosive and hazardous, limiting their use in cast-in-place scenarios [21]. Hence, there is a rising interest for "one part" or "just add water" AAMs as an alternative to PC-based blends. In their pioneering research, Duxson and Provis [22] highlighted the importance of developing one-part AAMs featuring adequate workability to achieve wider market acceptance. One-part AAMs show a two- to threefold reduction in environmental impact indicators (e.g., CO_2 emissions, energy use) relative to conventional two-part systems [7]. As their distinctive peculiarity, both solid alkali activators and aluminosilicates are prepared in a dry blend, and are activated only with water addition [23–25]. The activation reaction initiates as soon as the mix achieves a sufficiently high pH [6]. The reactive binders of one-part AAMs depend on several factors, including the dosage and type of activator, the solubility of solid activators, the mineral structure of the precursors, as well as curing and aging conditions. In AAMs, based on aluminosilicates mainly, Si–O–Al network structures are formed through polycondensation. When calcium-bearing precursors are included, such as GGBS, latent hydraulic phases like C–A–S–H are formed. Although both one-part and common AAMs involve similar reaction mechanisms, the high alkaline liquid environment in the latter systems generally promotes faster reactions compared to the former [7]. Nevertheless, the requirements of civil engineering applications necessitate a compromise in terms of reaction rate, which should impart sufficient plasticity for the transport, pouring and finishing of the in-situ applications, in addition to the mere evaluation of the mechanical properties. Therefore, a better understanding of one-part AAMs competing with Portland cement mortars in terms of fresh properties and setting time is essential.

So far, one-part AAMs have been investigated under various mixture design parameters at both ambient and elevated curing temperatures [26–29]. Ambient curing is regarded as a promising approach for cast-in-place applications while elevated temperature curing is more suitable for precast elements. As the main criticality, one-part AAMs are reported to set rapidly due to the heat generated by dissolved solid activators and chemical admixtures may be used to extend the setting time [30]. However, most of the common chemical admixtures are reported to lose effectiveness in highly alkaline conditions, resulting in a quick degradation of their functionality due to hydrolysis of the polymer side chains [31].

Another major challenge in the development of one-part AAMs is to optimize the amount of solid activator, i.e. sodium silicate. In fact, while a sufficient amount of solid activator is required to initiate the dissolution of the amorphous monomers provided by the precursors, overdosing of activators is reported to be inefficient as the reaction products rapidly precipitate on the unreacted precursors [32], resulting in hindered polymerization [20]. Moreover, higher activator contents result in a faster setting, as reported by Luukkonen et al. [7]. In addition, as the solid activator is one of the highest contributors to the carbon footprint of AAMs [33], it is of crucial interest to limit the fraction of sodium silicate in the mixes. Mastering the issue of limited setting time and corresponding workability [22], while achieving an optimal balance between sustainability

and performance, especially when using clay-based precursors [11], is critical to boost the massive production of one-part AAMs, reducing the demand of PC significantly.

The current study investigates the potential naturally occurring clays, referred to as low-grade clay in this research, which can be activated at ambient temperatures and one-part activators. This approach not only mitigates the environmental and safety concerns associated with conventional two-part activators but also enhances the sustainability and flexibility during production of AAMs by using more readily available and less costly precursor materials. Low-grade calcined clay, which is abundant in the Earth crust worldwide, was used in high volume in the mixture designs under investigation. However, low-grade clays as low reactive precursors often require the thermal treatment to boost the reactivity of the system, which can be eliminated by the addition of calcium rich alumino-silicates such as slags [34]. Therefore, critical influencing factors under investigation include tailored alkali activators and precursor formulations containing ground granulated blast furnace slag (GGBS) to address practical needs in the civil engineering. Clay minerals (calcined at 650 °C) were blended with slag in different ratios without resorting to chemical admixtures. To elucidate alkali-activation behavior, reaction kinetics were determined as a function of solid-activator dosage and precursor proportion, establishing dissolution, nucleation and reaction rate characteristics under ambient curing. Fresh performance was benchmarked against established practice for Portland-cement systems to enable equivalent performance assessment of fresh properties. Mechanical performance was measured over curing age to determine strength development and structural viability. Complementary microstructural, porosity and phase-evolution measurements were undertaken to identify pore-size refinement from capillary to meso ranges and changes in hydrate assemblages thereby corroborating the hydration kinetics and strength development.

2 Materials and methods

2.1 Materials

The raw clay used in this study was a low-grade multi-mineral clay containing ≤ 25 wt% kaolinite together with approximately 30 wt% mica, 18 wt% quartz, 11 wt% illite, 6 wt% chlorites, 5 wt% feldspar, 3 wt% calcite, and minor amounts of gypsum (1 wt%) and pyrite (1 wt%). The low-grade clay was industrially calcined at 650 °C and provided by Liapor GmbH & Co. KG, Hallerndorf, Germany. After calcination, the calcined clay (CC) exhibited an amorphous-rich structure with an amorphous content of approximately 65.7 wt% and a density of 2.6 g/cm^3. Ground granulated blast furnace slag (GGBS) has a density of 3.1 g/cm^3 provided by Dyckerhoff, Niederorschel, Germany. Quartz sand having a maximum size of 256.9 µm and water absorption capacity of 0.3% is used as the inert aggregate supplied by Strobel, Germany. In alkali-activated mortars, sodium disilicate (SS) with brand name of Sikalon® was provided from Wöllner GmbH, Ludwigshafen, Germany. SS was in solid form which favors the conditions for the one-part production as in similar in Portland cement products without additional preparation. Also, SS having a silica modulus of 2.1 is considerably user-friendly for the handling in AAMs [21]. SS had a maximum size of 500 µm (with an exceeding fraction < 5%) and a bulk density of 0.1 g/cm^3.

The physical properties of raw materials was measured by Laser diffraction particle analysis, LS 13–320 from Beckman Coulter. Particle size distribution (PSD) and other physical properties of raw materials is given in Table 1. The chemical compositions of CC and GGBS were determined via Energy-Dispersive X-ray spectroscopy while the properties of SS including its water content were obtained from the manufacturer's technical data sheet (Table 2). SEM micrograph images of binder materials are also shown in Fig. 1.

Table 1 Physical properties of the raw materials

Property	CC	GGBS	SS*	Sand
D_{V10}(µm)	0.7	0.8	n.a	111.1
D_{V75}(µm)	7.9	7.9	n.a	155.8
D_{V90}(µm)	26.6	32.5	n.a	210.0
Max. particle size (µm)	47.9	194.2	500	256.9
Density (g/cm^3)	2.6	3.1	0.1	2.6

*= *The properties of the solid activator (SS) are reported as declared by the manufacturer. For SS, the apparent density is known from the data-sheet*

Table 2 Chemical composition of raw materials and physical properties of CC, GGBS, and SS

Raw materials	SiO_2	Al_2O_3	Fe_2O_3	MgO	CaO	K_2O	Na_2O	H_2O
CC	47	25	9	3	9	4	–	–
GGBS	34	8	–	5	47		–	–
SS	56	–	–	–	–		28	16

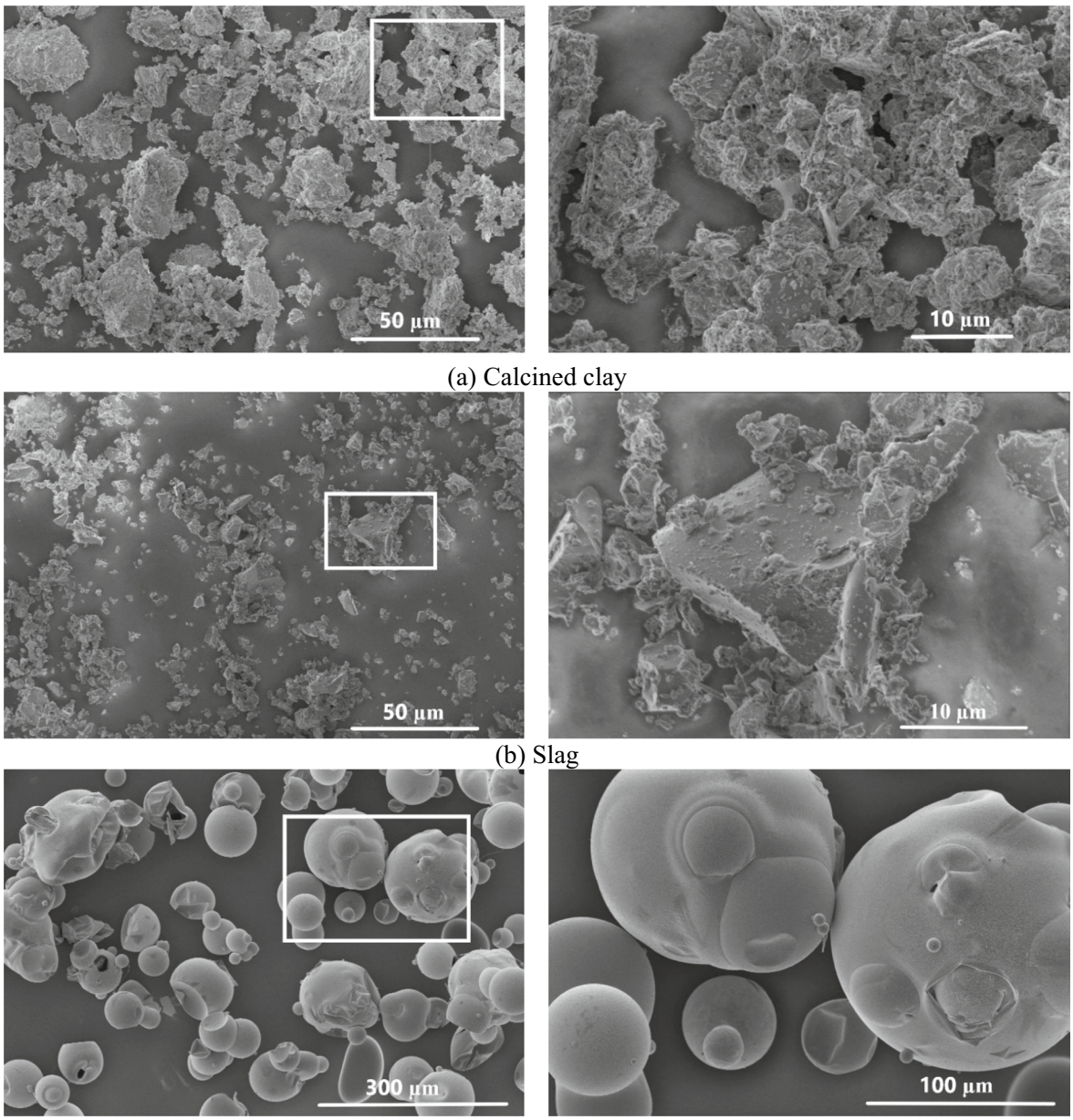

Fig. 1 SEM morphological images of (**a**) calcined clay (CC), (**b**) Slag (GGBS) and (**c**) Sodium disilicate (SS)

2.2 Mixture proportions

Mixture proportions were investigated according to two parameters, i.e., solid activator concentration and precursors. The rationale for addressing these two parameters is to reach a balance between workability, setting time and mechanical strength of AAM mixtures, to be applied as scalable construction materials. The mixture proportions and test parameters are presented in Table 3.

To ascertain the role of calcined clay in blended AAMs, two blends with different CC/GGBS ratios, namely 0.81/0.19 and 0.63/0.37, at a constant solid activator ratio of 0.22 were investigated at ambient curing and compared with a mix including only CC as the precursor. The corresponding alkali-activated mortars were denoted as SS/CC81, SS/CC63 and SS/CC100. The spotlight is set on maximizing the use of CC in AAMs [16], while the addition of minor GGBS fractions is intended to mitigate the slow reactivity of low-grade CC at ambient curing temperature, which are reported to entail long setting times and lower mechanical properties.

2.3 Mixture procedure and specimen manufacturing

Due to the high water demand of calcined clay [35] and in order to prevent the fast dissolution of the solid activator upon the addition of water [14, 36], the solid binder phases were initially dry-mixed to promote contact between the precursors and the activator, excluding inert aggregates. Water and fine aggregates were incorporated stepwise at a later stage, according to the following mixing procedure: (i) calcined clay, GGBS and solid sodium disilicate powder were dry-mixed using a 5L-planetary mixer HSM20 from Hobart (Offenburg, Germany) for two minutes at 140 rounds per minute (rpm); (ii) after that, water was gradually added within one minute; (iii) then, the fresh mixtures were stirred at constant speed rates of 140 rpm and 285 rpm for five and two minutes, respectively; (iv) finally, fine sand was added within 30s and the mortar was mixed for further two minutes.

The fresh mixtures were poured into prism molds ($40\times40\times160$ mm^3) and left to cure for 3 days under standard laboratory conditions (65 ± 5% relative humidity (RH), 20 ± 2 °C) before being demolded and cut into cubic specimens with of 40 mm side. The cubes were wrapped into plastic bags and stored in a climate chamber at (20 ± 2 °C) until the target testing ages (7, 14 and 28 days).

2.4 Testing

2.4.1 Reaction kinetics of clay-based AAMs

The reaction kinetics of the of AAM pastes were determined using an IC TAM Air calorimeter from TA Instruments (USA) at 20 °C. Current knowledge indicates that alkali activation comprises the following steps: (i) dissolution of precursors, (ii) speciation of aluminates and silicate source, (iii) gelation, (iv) reorganization and polymerization and (v) hardening [13]. Along with the formation of these aluminosilicate gels, calcium alumina silicate hydrates are also formed in calcium-bearing AAMs mixtures. As these phases are required to be completed before reaching a comprehensive understanding of the reaction kinetics [37, 38], the heat release generated from the pastes was monitored for at least ten days. Samples were mixed externally, transferred into 7-g calorimeter glass bottles containing the fresh mixture, and immediately sealed before being loaded into the IC channel. The reported value was normalized by mass.

Table 3 Mixture proportions of clay-based one-part AAMs (by mass)

Mixture ID	CC/ precursor	GGBS/ precursor	SS/ binder	W/ binder*	Sand/ binder	Parameter
SS19/CC81	0.81	0.19	0.19	0.39	0.5	solid activator (SS)
SS22/CC81	0.81	0.19	0.22	0.37	0.5	
SS25/CC81	0.81	0.19	0.25	0.35	0.5	
SS/CC100	1.00	0.00	0.22	0.38	0.5	precursors (CC and S)
SS/CC81	0.81	0.19	0.22	0.38	0.5	
SS/CC63	0.63	0.37	0.22	0.38	0.5	

*=Ratio of W/B refers water to precursors (CC+GGBS) and solid activator (SS)

2.4.2 Fresh properties

Setting time and flowability of the paste and mortar mixtures were assessed. The initial and final setting times of the fresh pastes were determined using a Vicat's apparatus in conformity with the ASTM C807 standard [39] and results were compared with the corresponding setting time requirements defined for PC-based counterparts. The flowability of the pastes and corresponding mortars was measured with a Hägermann flow table according to the EN 1015–3 [40].

2.4.3 Hardened properties

The compressive strength development of the various one-part AAMs mortars was evaluated using cubic specimens with dimensions of $40\times40\times40$ mm^3. For each variant, six identical specimens were tested for each curing age, namely of 7, 14 and 28 days. The tests were performed using a universal hydraulic machine set at a loading rate of 0.5 N/mm^2 per second.

2.4.4 Analytical investigations

Analytical investigations were performed on mortar specimens after 28 days of curing to characterize their morphology and chemical composition. The pore size distribution of the specimens at the hardened state was evaluated by means of a mercury intrusion porosimeter (MIP, PASCAL 140/440, Thermo Fisher Scientific Inc., Italy) to correlate with the mechanical results. A minimum of 3 fragments of each mixture, with a mass of approximately 5 g, were analyzed setting a pressure range of 0 to 400.71 MPa. Finally, the morphology of the fracture surfaces were examined using a scanning electron microscope (SEM, Quanta 250 FEG from Bruker FEI, Eindhoven, the Netherlands) set at 10 kV of operating voltage and 40 Pa pressure. Thermogravimetric analyses (TGA) were carried out using a STA 409 cell device from Netzsch, Germany. The paste specimens without sand were heated from 20 to 1000 °C at a heating rate of 10 K/min in an oxygen environment (60 ml/min O_2 gas flow). As TGA was mainly used for a comparative evaluation of dehydration/decomposition behavior rather than for precise phase identification or quantitative phase analysis, a stable oxidizing environment was selected. Prior to testing, all samples were treated in isopropanol for at least 24h to stop the reaction, followed by drying in a vacuum desiccator for 7 days.

3 Results and discussion

3.1 Alkali activation kinetics

3.1.1 Effect of alkali activator

Understanding the reaction kinetics is pivotal in designing AAMs to optimize both their workability and mechanical properties. The effect of different sodium disilicate ratios on the reaction kinetics of the clay-based one-part AAMs is presented in Fig. 2. When water is added to one-part mixtures, the solid SS dissolves, triggering an exothermic reaction [41]. Irrespective of the SS concentration, the initial dissolution peak was narrow, followed by a short dormant period akin to the induction period in PC hydration. Indeed, with higher SS concentration the w/b ratio is slightly reduced which increases the relative alkali concentrations. The subsequent reaction leads to the second peak, which is related to the earlier formation of (C/N)–A–S–H [7].

As can be seen in Fig. 2b, the cumulative heat released by the mixture with 25% of solid activator was 9.0% and 27.7% higher than its counterparts with 22% and 19% of sodium disilicate, respectively. In fact, higher concentrations of sodium disilicate favor a faster alkali activation, as evidenced by the faster increase in cumulative heat release and the broadening of the second heat peak. However, the reactions were not finished yet, as seen in the further ascending branches of the plots. Although further analysis is required, this finding correlates with the initial setting time, which is found to increase when higher dosages of solid activator (SS25/CC81) are included, as elucidated in subsequent sections. In addition, the strength development tends to be less pronounced by higher solid activator doses, as examined in the following sections.

3.1.2 Effect of precursor

To pinpoint the influence of the substitution of CC by GGBS, Fig. 3 plots the isothermal calorimetry curves for the mixtures with the same activator dosage (22%) and with different amounts of CC and GGBS. As

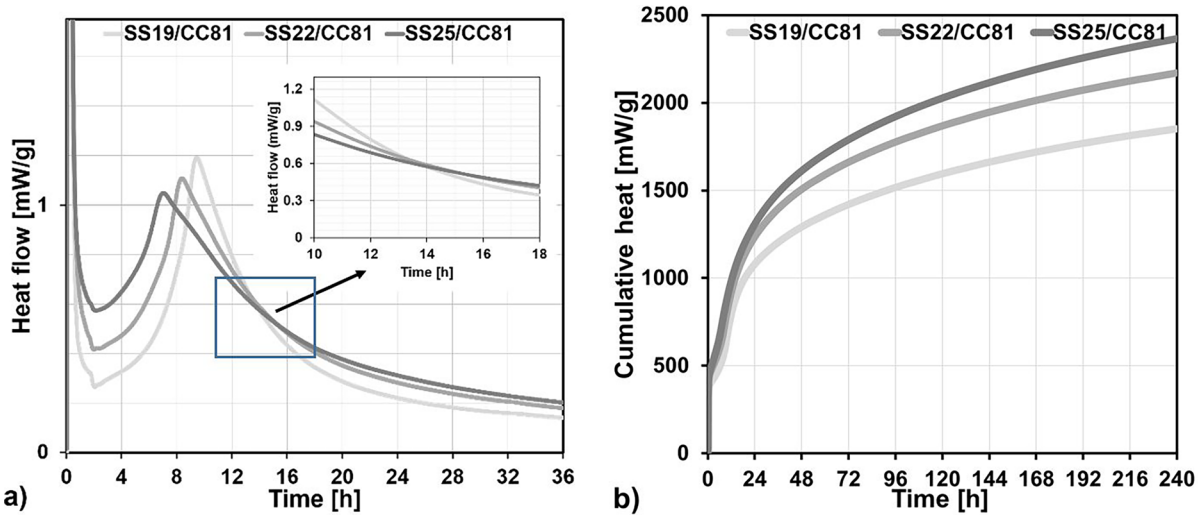

Fig. 2 Heat flow (**a**) and cumulative heat (**b**) of the AAM mixtures: effect of alkali activator

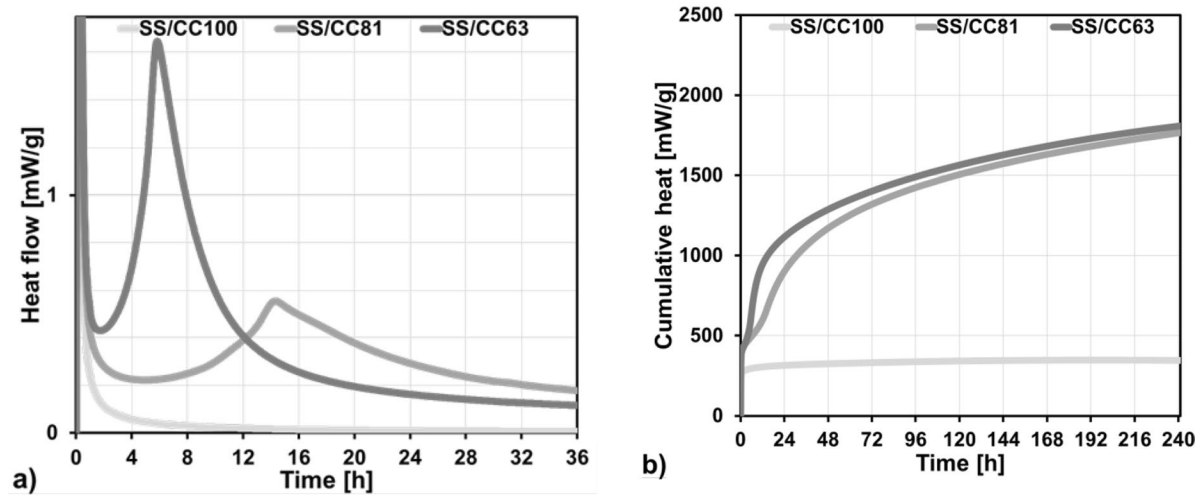

Fig. 3 Heat flow (**a**) and cumulative heat (**b**) over time of the AAM mixtures: effect of precursors

evident in Fig. 3, the mixture including CC alone (SS/CC100) showed no peak at 20 °C. This phenomenon aligns with the behavior of low calcium-bearing precursors at ambient curing conditions (around 20 °C), underscoring the temperature dependence of curing 100% calcined clay mixtures [7]. On the contrary, the utilization of 19% and 37% latent hydraulic slag led to the emergence of a second peak in the curve of the heat flow within the first 36h.

In the given results (Fig. 3a), the highest secondary peak was recorded as 1.65 mW/g for the SS/CC63, being almost three times than the SS/CC81 counterpart (0.55 mW/g), highlighting the significantly higher activation of the former. Notably, an almost twofold increase in amount of GGBS resulted in a threefold increase of the second peak, which may be related to extensive hydration and polymerization of products such as C–(A)–S–H or N–A–S–H [42, 43]. This delayed, broader and less intense acceleration peak of the paste with 19% GGBS (SS/CC81), compared to the counterpart with 37% GGBS (SS/CC63), can be attributed to a diluted Ca-containing mixture

[44]. In addition, the higher dosage of slag considerably shortened the induction period and contributed to a faster onset of the second peak. This effect gradually declined with increasing age (Fig. 3b).

In fact, the cumulative heat measured from SS/CC81 and SS/CC63 mixtures after 10 days is almost equalized (only 2% higher for the latter), whereby both systems show still an ongoing reaction as seen in steady increase in cumulative heat which can be attributed to the continuous dissolution, gradual formation of dissolved species and polymerization within the gel network [5]. These results indicate that the slag content in one-part AAMs can be effectively reduced. In fact, the longer curing time may provide a similar activation capacity, opening the way for tailoring the composition of clay-based AAM blends for cast-in-place or additive manufacturing applications with additives such as GGBS, which act as a calcium-rich admixture to create favorable conditions for low-calcium precursors at 20 °C.

3.2 Workability of AAMs

Figure 4 displays the average flowability of the mixes in terms of spread diameter, focusing on the two previously identified criteria. All mixtures show high repeatability with only minimal standard deviations (0.2–0.3 cm).

As can be seen, increasing the alkali activator fraction did not reduce the flow diameter of the blends, unlike several studies where higher activator dose was reported to reduce the flowability of the mixtures [45–47]. On the contrary, the increased water content of the mixture due to the bound water of SS may have favored the slightly higher flowability for the SS22/CC81 (17 cm) and SS25/CC81 mixtures (17.2 cm) compared to SS19/CC81 (12.5 cm).

In general, it is known that the type and the ratio of the solid activator plays a prominent role in the fresh properties of AAMs [48]. Our findings can be directly attributed to the nature of sodium disilicate, which possesses a viscous characteristic, as also reported by Bature et al. [49], when calcined clay was used in combination with a sodium silicate solution. Considering the effect of precursor type, the use of GGBS reduced the flow diameter of the mixtures, due to the irregular plate-like particle morphology and in particular due to the high calcium oxide (CaO) content [45, 50]. It is noteworthy that the workability for the mixture with the highest slag content (37% by weight of total binder) was still comparable to those of ordinary cement based mortars [49], and although

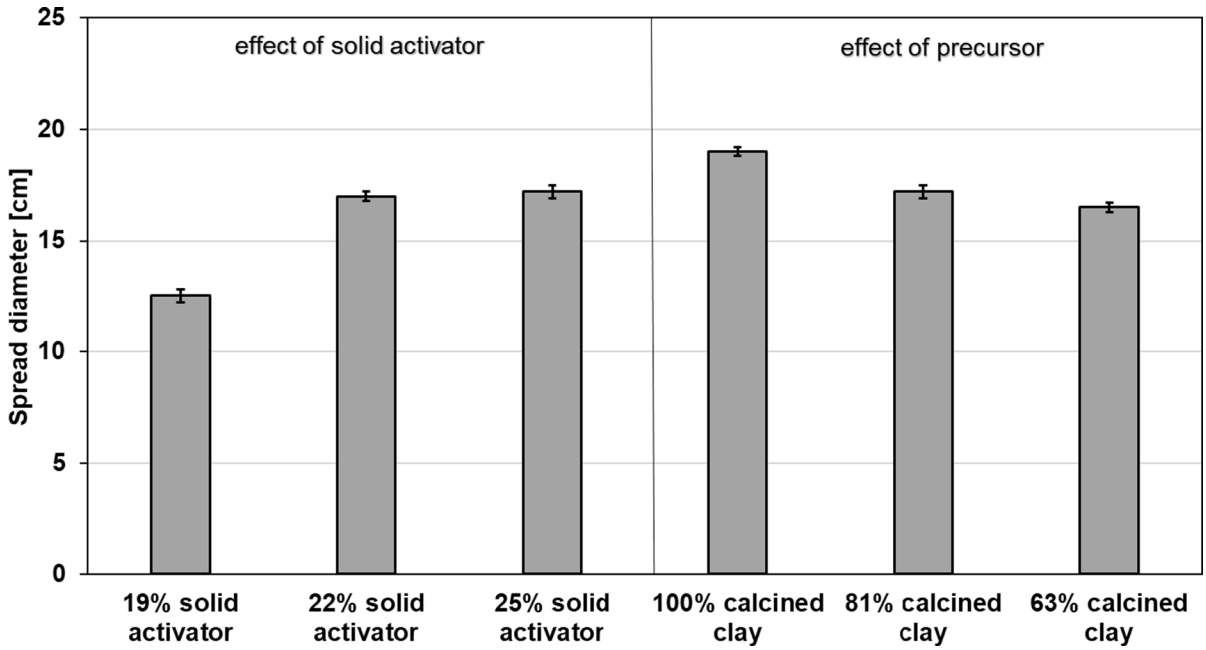

Fig. 4 Flowability of the different alkali-activated mortars

the liquid/binder ratio is generally adjusted to tailor the flow spread of the mixes [46], our results indicate that an adequate workability can also be achieved by adjusting the amount of solid activator and precursor. It should also be emphasized that the present study intentionally focused on chemical additive-free one-part AMMs incorporating high volumes of low-grade calcined clay under ambient curing conditions which remains a challenging approach in terms of fresh-state stability and workability retention. Nevertheless, the obtained flowability results indicate that acceptable fresh properties can still be achieved through precursor and solid activator optimization. Future studies may further investigate workability evolution over extended periods relevant to practical applications such as precast and ready-mixed concrete production.

3.3 Setting time of mixtures

One of the main known drawbacks of one-part AAMs lies in their short initial setting time, which makes these formulations often unsuitable for real-world, large-scale applications [7]. To compete with Portland cement, a one-part AMM should feature an initial setting time greater than 45 min, while the final setting time should not exceed 375 min, according to ASTM C150 [51]. Chemical admixtures such as sodium tetraborate decahydrate-borax ($Na_2B_4O_7 \cdot 10H_2O$), citric acid, phosphoric acid solution (H_3PO_4), sodium triphosphate ($Na_5P_3O_{10}$) have been proposed to extend the initial setting time of AAMs [52], although their use still requires deeper understanding [7] due to their sensitivity to the highly alkaline conditions of AAMs [31]. However, the setting time can also be optimized through the adjustment of precursor and activator rather than only the w/b ratio, enhancing reproducibility. As shown in Fig. 5, the alkali activator was influential in setting time after a certain dosage.

A higher solid activator fraction (SS25/CC81) yields in a prolonged initial setting (47 min) and reduced final setting (91 min), compared to SS19/CC81 and SS22/CC81, which recorded similar initial and final setting times. For a given water content, the increase in initial setting time with higher amount of solid activator is basically related to the gradual dissolving ability of a higher amount of alkali activator as sodium disilicate has coarser particles compared to CC and GGBS used in this study. Hence, a high amount of activator precipitated around unreacted compounds that could impeded further reaction, resulting in a delayed initial setting time [37]. Indeed, the prolonged initial setting time and reduced final setting time of the mixture with the highest solid

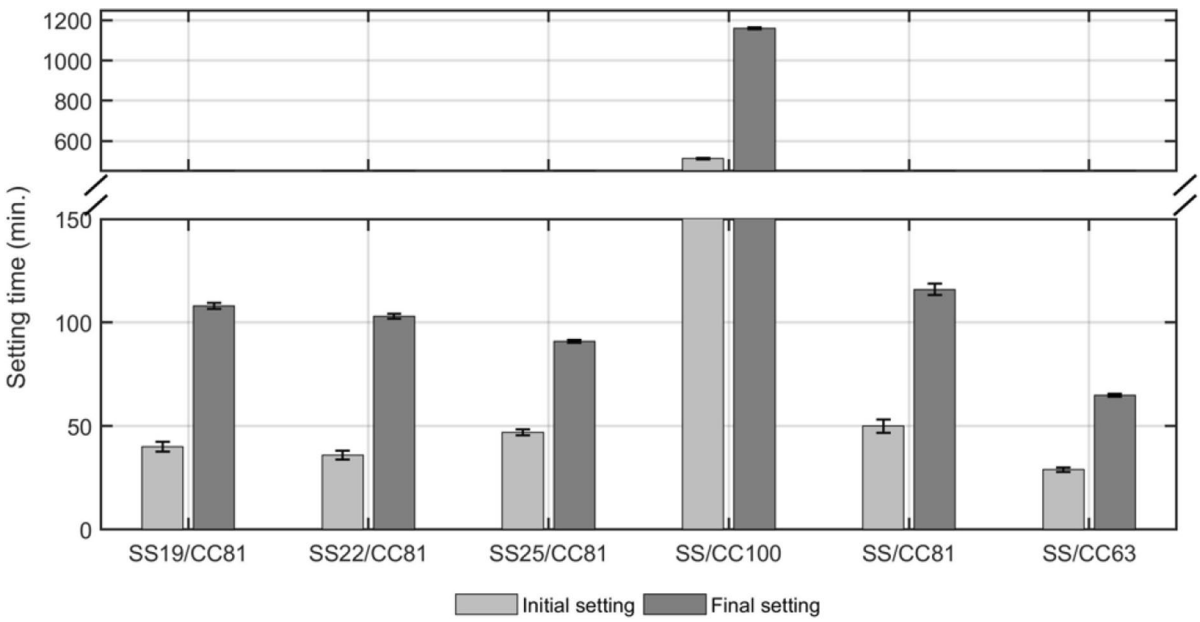

Fig. 5 Setting times of the different alkali-activated mortars

activator dosage (SS25/CC81) are closely related to the lower secondary peak and higher total cumulative heat release shown in Fig. 2, respectively.

On the other hand, the quantity and type of precursor had a more straightforward effect on the setting time, as also seen in the IC experiments. The partial replacement of CC by GGBS significantly reduces both the initial and final setting times. This fact is to the faster dissolution and hydration reaction of CaO than SiO_2 and Al_2O_3 [53]. However, an excessive dosage of slag results in a shorter setting and rapid hardening, as seen for SS/CC63. On the other hand, the 100% calcined clay AAM paste (SS/CC100) had a considerably longer initial (512 min) and final setting time (1160 min), which is well beyond the requirements for cement binders [39] and is not relevant to be shown in Fig. 5. This is due to the very limited dissolving capacity of Si and Al monomers at room temperature, which would instead require a high activation energy to accelerate the reaction [53, 54].

Considering the final setting time, all suitable blends stood well below 375 min and in compliance with the PC standard [39, 55]. Remarkably, the SS25/CC81 and SS/CC81 mixes were also within the standard requirements for initial setting time according to ASTM C150. Based on the trade-off between workability/setting time and hydration kinetics, one-part clay-based AAM mixtures can be successfully produced at ambient curing without the need for chemical admixtures.

3.4 Compressive strength

3.4.1 Effect of solid activator

The SS19/CC81, SS22/CC81 and SS25/CC81 mixtures exhibited average compressive strengths of 13, 21 and 24 MPa, respectively, after 7 days when increasing sodium disilicate ratios were used. As shown in Fig. 6, the average compressive strengths of these mixtures increased at 28 days of curing to 26 MPa for SS19/CC81, 38 MPa for SS22/CC81 and 40 MPa for SS25/CC81.

Increasing the sodium disilicate content led to higher compressive strength at all curing ages. However, the percent increase in strength decreased beyond 7 days. The lower increase rate of blends with higher sodium disilicate may be related to the inhibition of the coagulation of gel synthesis in the presence of an excessive amount of activator [20, 32]. While an increased ratio of solid activators contributed to higher compressive strengths, the ongoing reaction may have been hindered due to limited diffusion of dissolved species [52]. Further addition of activator contributed to strength to a lesser extend, as the 28-day cured SS19/CC81, SS22/CC81 and SS25/CC81 blends had 99%, 84%, and 67% higher compressive strength, respectively, than their 7-day cured counterparts (Fig. 6b). In this regard, blends containing 81% calcined clay demonstrated satisfactory compressive strength (24–40 MPa), which may be of

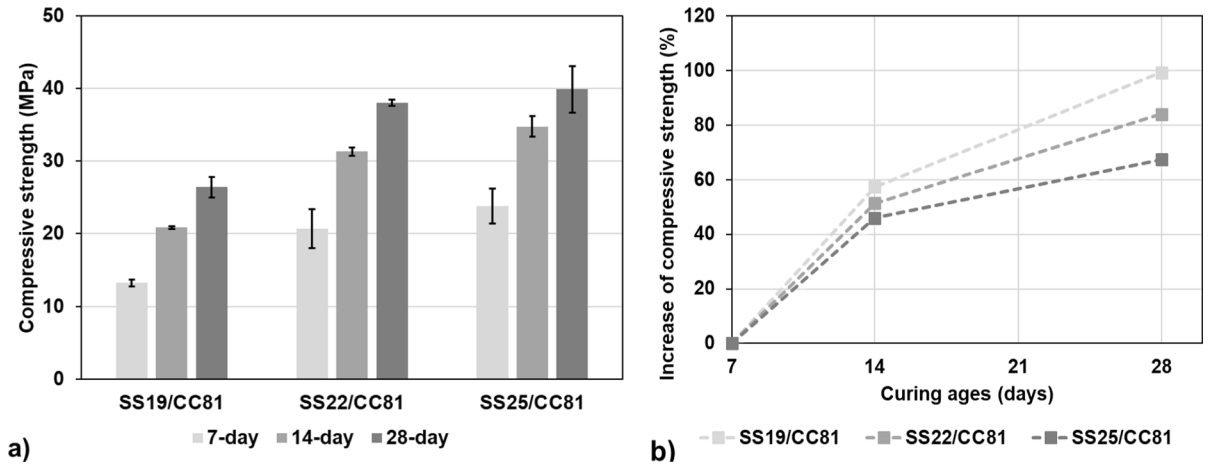

Fig. 6 Compressive strength of the alkali-activated mortars: **a** effect of solid activator, **b** corresponding percental increase of compressive strength (%) with aging

interest for general-purpose cast-in-place applications in civil engineering.

3.4.2 *Effect of precursors*

The average compressive strength values along with their scatter for all tested groups are given in Fig. 7, highlighting the effects of the precursor parameters.

At 7 days, results were 2.5, 29 and 37 MPa for the mixtures SS/CC100, SS/CC81 and SS/CC63 comprising 0%, 19% and 37% slag, respectively. At 14 and 28 days, the compressive strength of the SS/CC100 mixture remained nearly constant at around 2.6 MPa, while the SS/CC81 and SS/CC63 mixtures exhibited mean compressive strength ranging from 33 to 40 MPa and from 39 to 52 MPa, respectively. Hence, the effect of the calcined clay substation with GGBS results clearly in an increase of compressive strengths. These results indicate that a specific amount of latent hydraulic species is necessary to promote the reaction at ambient temperature, as similarly reported for instance for fly ash-slag blended system [56].

In the case of calcium-free binders (SS/CC100) no adequate compressive strengths were obtained ambient temperature. As shown in Fig. 7b, a lower percent increase in compressive strength for blends with higher GGBS content can be attributed to their relatively lower alkali modulus [57, 58]. As the calcined clay content increases from 63 to 81%, the low activator modulus may have benefited from the reaction process of Si and Al, resulting in a slightly higher percent increase in compressive strength [59].

The results clearly emphasize that the slag-to-binder ratio has a significant influence on the compressive strength of mixes. However, the relatively moderate increase in strength with higher GGBS incorporation suggests that the role of GGBS in the present system is primarily associated with enabling ambient-temperature activation rather than solely maximizing compressive strength. This observation is also consistent with the calorimetry results where the SS/CC100 mixture exhibited very limited heat evolution, on the other hand, even relatively low slag incorporation significantly increased the reaction kinetics and cumulative heat release under ambient curing conditions. In addition to the slag contribution, minor filler and nucleation effects associated with calcite-containing phases may also have contributed to the observed strength trends. The amorphous phase of the latent hydraulic slag is highly reactive in alkaline environments, such as those created by sodium disilicate yielding higher compressive strengths. These alkaline activators raise the pH, promoting the dissolution of the slag's amorphous phase and facilitating the formation of strength-giving reaction products like C–(A)–S–H or N–A–S–H gels. Nevertheless, balancing the satisfactory compressive strength and the sustainability constraints, low amount of slag, i.e., AAM/CC81 blend would be recommended. Accordingly, the function of slag is not only a strength contributor but also a kinetic activator in the

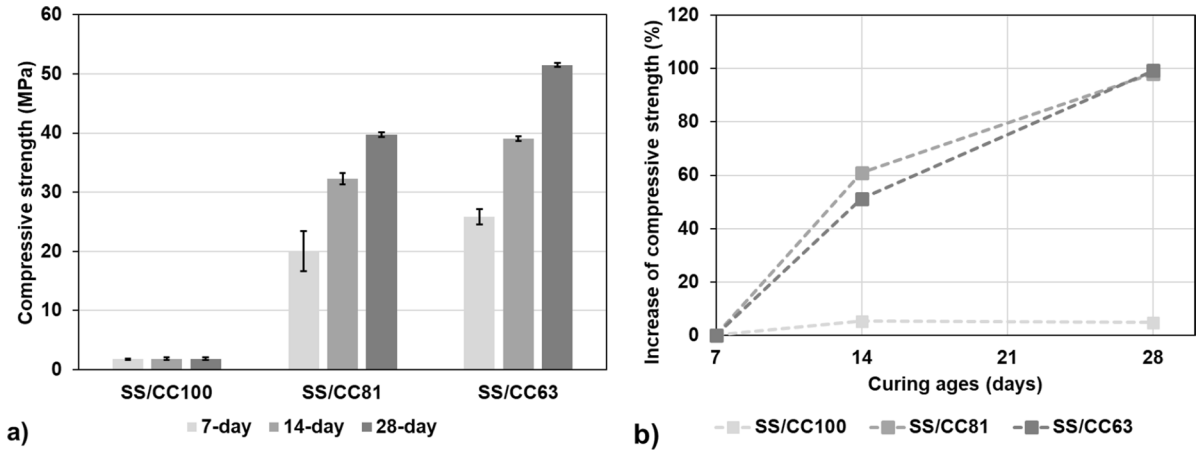

Fig. 7 Compressive strength of the alkali-activated mortars: **a** effect of slag, **b** corresponding percental increase of compressive strength (%) with aging

clay-dominant one-part system. Its limited incorporation supplies calcium-rich species that enable dissolution at ambient temperature fostering the formation of hybrid gels that bridges the reactivity gap of low-calcium clays. This balanced gel network accelerates setting and enhances microstructural cohesion without compromising workability. Accordingly, a low-slag and clay-dominant formulation provides the optimal compromise between reactivity and strength development as well as sustainability producing a binder that hardens effectively under ambient conditions while preserving its practical handling and low environmental footprint.

3.5 Microstructure of clay-based one-part AAMs

3.5.1 Pore size distribution of mixtures having different solid activator

Figure 8 showcases the effect of sodium disilicate dosage on the pore size distribution and refinement at the hardened state of different AAM blends with constant calcined clay content (81%) at 7 and 28 days.

After a further 21 days of ambient curing, all specimen showed a significant refinement in their pore sizes, explaining the increase in compressive strength as previously indicated. In addition to Fig. 8, a more detailed view and a classification of the pore size distributions is presented in Table 4, according to Zeng et al. [60].

In general, as higher use of SS yields in a reduction of the total porosity which is in good agreement with the oberservations made in isothermal calorimetric and mechanical analysis. Also, all specimen showed a clear pore refinement from the 7th to the 28th day of reaction. With lower SS content (SS19/CC81 and SS22/CC81), macropores and larger pores were notably reduced. In contrast, the SS25/CC81 blend showed some degree of pore size refinement only at the mesopore scale. Thus, the reduction in larger pores due to the longer curing time may have had a greater impact on the strength development.

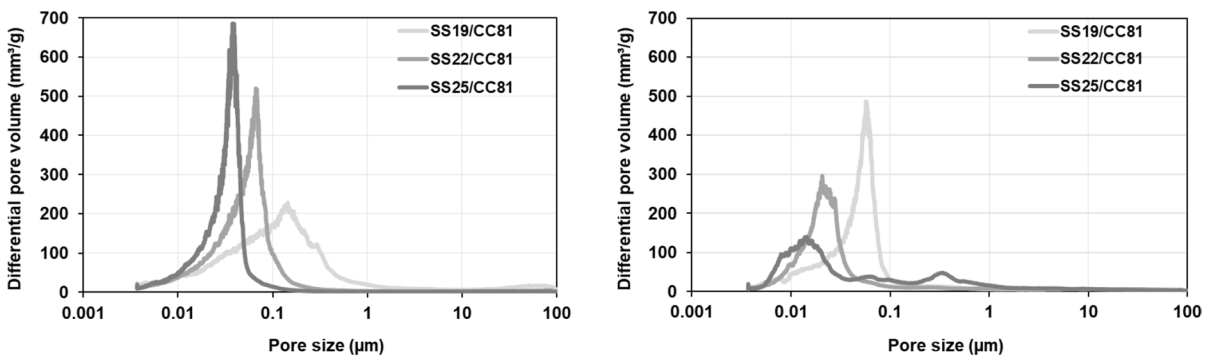

a) Differential pore volume (7 days)

b) Differential pore volume (28 days)

Fig. 8 Effect of solid activator on the pore size distributions of the mixtures by MIP measurements

Table 4 Effect of solid activator on the porosities obtained by MIP

Blend ID	SS [%]	Curing age [days]	Nano-pores (3–10 nm) [vol%]	Mesopores (10–50 nm) [vol%]	Macropores (50–200 nm) [vol%]	Larger pores (> 200 nm) [vol%]	Total MIP porosity [vol%]
SS19/CC81	19	7	1.8	8.4	16.3	10.8	37.3
SS19/CC81		28	1.7	13.2	13.1	2.9	30.9
SS22/CC81	22	7	1.6	13.8	16.7	1.8	33.9
SS22/CC81		28	2.2	19.0	1.8	3.6	26.5
SS25/CC81	25	7	1.9	27.0	2.3	1.0	31.9
SS25/CC81		28	3.7	10.3	3.3	6.6	23.9

Additional analysis of the morphology of the blends was carried out by SEM, confirming the MIP data and mechanical performance. For example, a more porous microstructure was observed in the surface morphology of the SS19/CC81 specimen, compared to SS22/CC81 and SS25/CC81, as shown in Fig. 9.

Clearly, varying amounts of unreacted sodium disilicate were detected. Unreacted solid activator particles of larger size can be seen in Fig. 10, which shows lower magnification SEM images of the blends and reveals that higher sodium disilicate fractions result in a more numerous undissolved particles. On the other hand, more reaction products induced by the increased use of solid activator has compensated for the larger pores, showing higher strength at all curing ages for SS25/CC81 compared to SS22/CC81 and SS19/CC81.

3.5.2 *Pore size distribution of mixtures having different precursor*

Figure 11 shows the effect of the precursor mix on the pore size distribution of AAM binders and Table 5 gives the according pore classifications.

Between 7 and 28 days, all blends underwent a significant pore size refinement, explaining the observed improvement in compressive strength. However, the influence of GGBS content on the total pore volume is not clear, as SS/CC100 and SS/CC63 exhibited similar total porosity at 28 days. In fact, the slag-free specimen (SS/CC100) is characterized by clustered, unreacted calcined clay particle, resulting in a

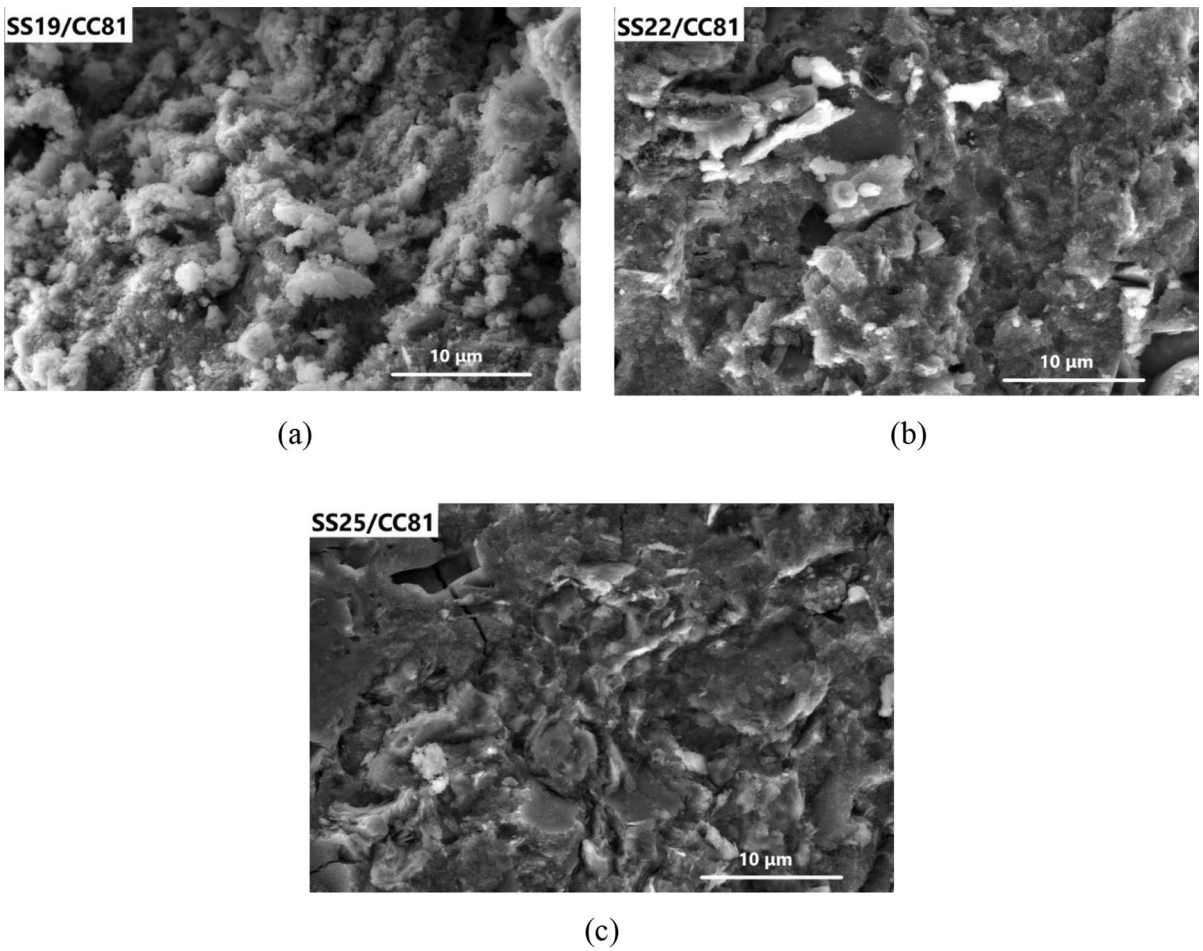

Fig. 9 Surface morphologies of clay-based AAM mixtures having different amounts of solid activator

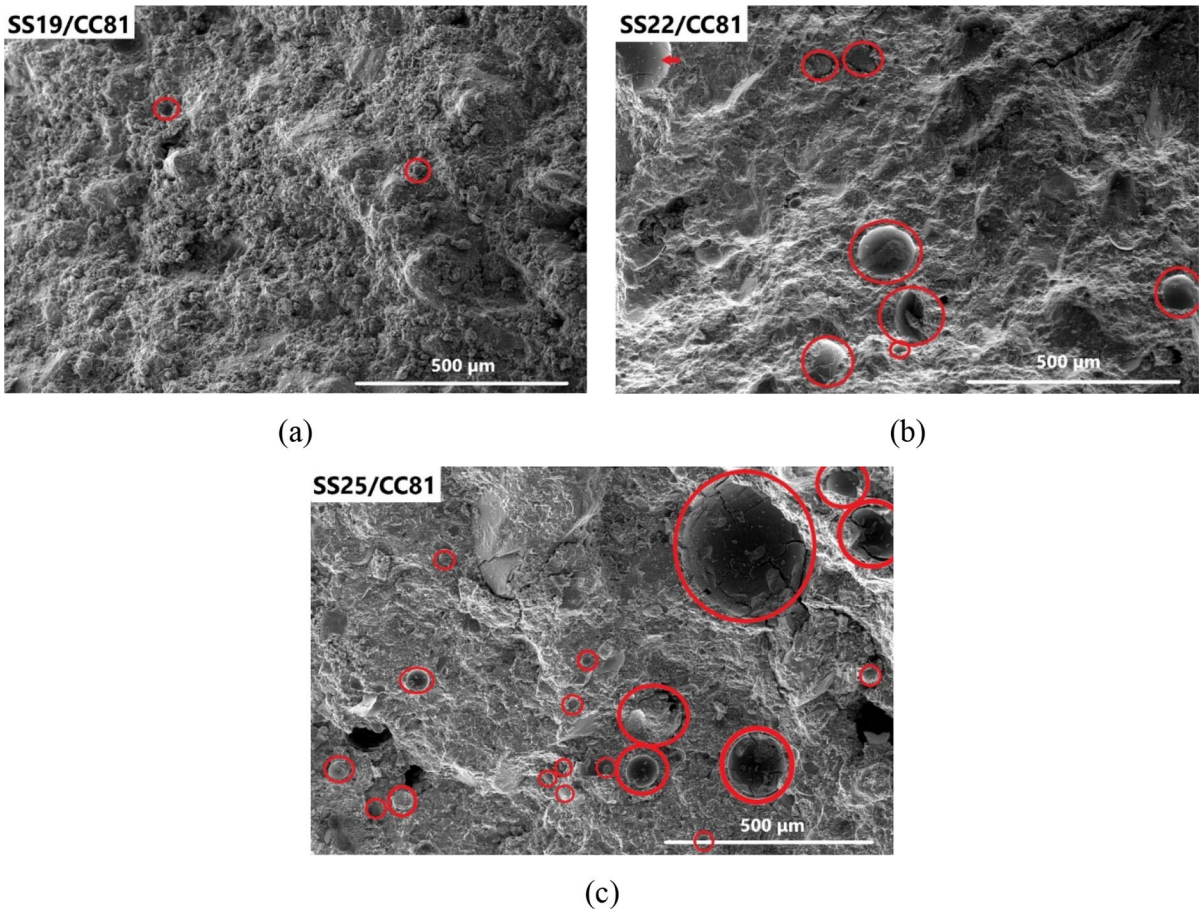

Fig. 10 Higher degree of undissolved solid activator for mixtures in the order of: SS25/CC81 > SS22/CC81 > SS19/CC81

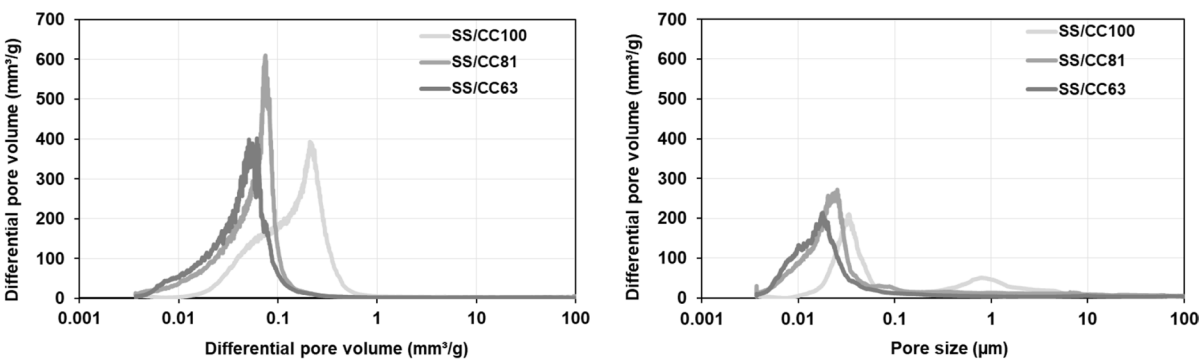

Fig. 11 Effect of precursor on the pore size distributions of the mixtures by MIP measurements

Table 5 Effect of precursor on the porosities obtained by MIP

Blend ID	CC fraction [%]	Curing age [days]	Nanopores (3–10 nm) [vol%]	Mesopores (10–50 nm) [vol%]	Macropores (50–200 nm) [vol%]	Larger pores (> 200 nm) [vol%]	Total MIP porosity [vol%]
SS/CC100	100	7	0.3	5.0	18.3	13.2	36.9
		28	0.2	11.4	2.4	9.6	23.6
SS/CC81	81	7	1.6	12.6	19.3	1.7	35.3
		28	3.2	17.3	2.4	4.9	27.8
SS/CC63	63	7	2.1	17.3	12.6	1.4	33.3
		28	4.5	14.6	1.6	2.4	23.2

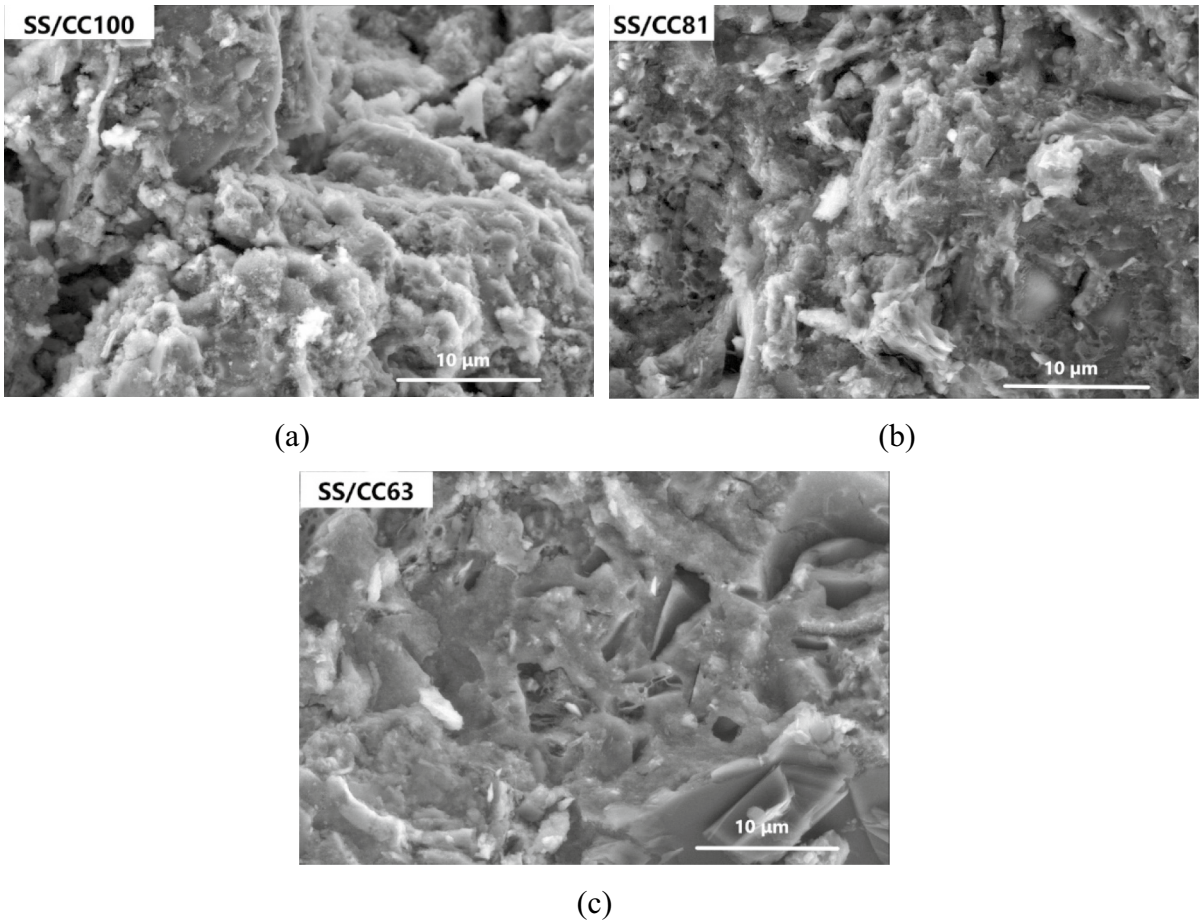

Fig. 12 SEM images of clay-based AAM mixtures having different precursor ratios

less compacted microstructure (as shown in the SEM micrograph in Fig. 12). Hence, the reduced mechanical performance of SS/CC100 is mainly explained by the predominant larger porosity (> 200 nm), as compared to that of slag-containing mixtures.

By increasing the GGBS dosage, a refinement of the pore structure was observed, particularly in the range of macropores (50–200 nm), which is in agreement with studies using slag with metakaolin or fly ash [61–63]. This distinction can be attributed to

the heir corresponding reaction mechanisms within the alkaline environments. The high-CaO containing slag promotes the formation of C–(N)–A–S–H gels, resulting in a more compact microstructure and reduced pore size [64]. Focusing on the SEM micrographs in Fig. 12, higher amounts of slag resulted in a more pronounced amorphous gel morphology, as also reported in literature [65].

3.5.3 Thermal decomposition behavior of mixtures having different solid activator

Figure 13 reveals the thermal analysis of the AAM blends activated with different ratios of sodium disilicate at 7 and 28 days.

For both curing ages, each mixture underwent a mass loss up to 200 °C, mainly associated with the evaporation of physically bound, interlayer and gel-associated water retained within the formed reaction products and microstructure. [65]. Further mass loss was observed between 200 and 700 °C, which can be divided into two distinct temperature ranges to better analyze the decomposition of different gel phases. Firstly, within 200–400 °C, the mass loss in this range is primarily due to the decomposition of C–A–S–H and N–A–S–H gels. The SS19/CC81 mix displayed the least mass loss during this phase at both 7 and 28 days, indicating a limited extent of C–(A)–S–H formation and possibly lower N–A–S–H gel content. In contrast, the SS22/CC81 and SS25/CC81 mixtures exhibited higher mass losses, suggesting a more significant formation of N–A–S–H, contributing to higher reaction degrees. Temperature between 400–600 °C reflects the decomposition of C–A–S–H gels and further breakdown of N–A–S–H. Again, SS19/CC81 showed minimal mass loss, indicating limited gel formation. The results may also suggest that the reaction development in SS25/CC81 is more time-dependent compared to the other mixtures. Although, the low-temperature mass loss behavior at 7 days remained relatively limited, the increased dehydration observed after 28 days may indicate

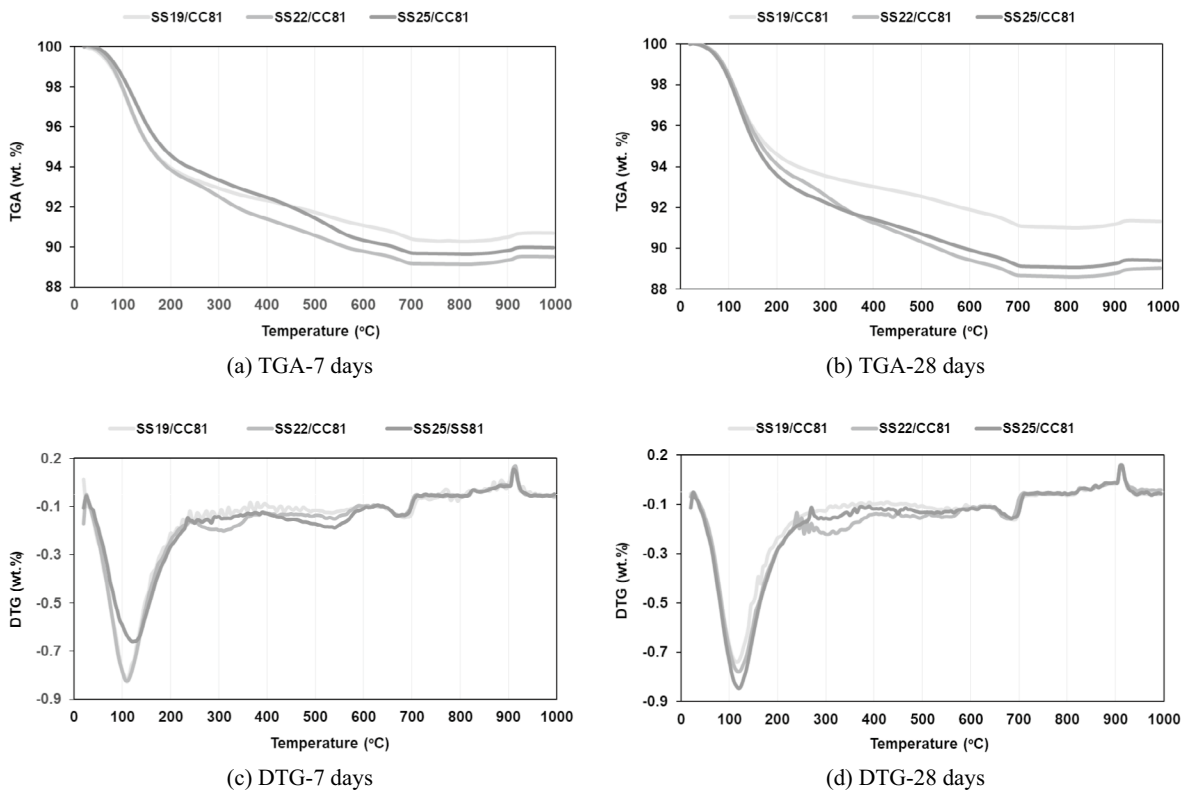

(a) TGA-7 days

(b) TGA-28 days

(c) DTG-7 days

(d) DTG-28 days

Fig. 13 TGA/DTG curves of clay-based AAMs having different activator content at different ages

progressive gel formation and evolving aluminosilicate reaction products at higher activator contents under ambient curing conditions. Ultimately, all mixtures appeared to be thermally stable beyond 700 °C.

3.5.4 Thermal decomposition behavior of mixtures having different precursor

The presence of GGBS played a major role in the thermal response of the AAM blends, as shown in Fig. 14.

The slag-free SS/CC100 binder exhibited only 6% and 8% mass loss at 7 and 28 days, respectively, up to 1000 °C, while the blends containing GGBS featured higher mass loss at both curing ages. In addition, the thermal decomposition process of the 28-day cured SS/CC81 and SS/CC63 was almost identical, with the initial evaporation of physical water and chemically bound water occurring up to about 200 °C.

The lower mass loss observed for the slag-free mix is explained by the lower degree of reaction and only limited formation of geopolymer gel and the absence of hydrated C–A–S–H phases. In the case of the binary blends, SS/CC81 and SS/CC63 had considerably accelerated mass loss up to 300–350 °C, which is associated to the loss of chemically bound water from the formed C–A–S–H gel [64] induced by the CaO rich slag [66].

4 Conclusion

The present paper examines the results of a comprehensive investigation aimed at addressing the major limitations of AAMs, such as the need for additional thermal curing, harmful liquid activators and the scarcity or regional dependence of precursors. Specifically, one-part clay-based AAM mortars were designed without the use of chemical admixtures and cured under ambient conditions, considering two main mix-design parameters, i.e. the dosage of solid activator (sodium disilicate) and the content of calcined clay, as a widely available low-calcined

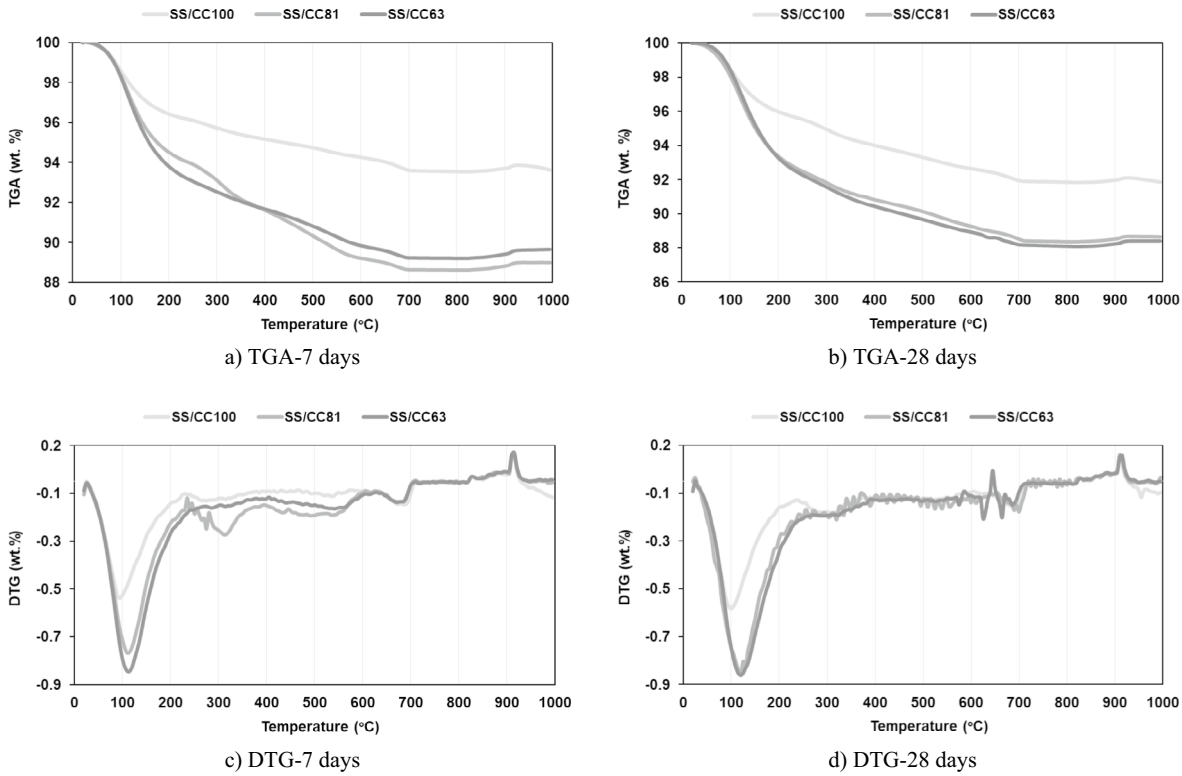

a) TGA-7 days

b) TGA-28 days

c) DTG-7 days

d) DTG-28 days

Fig. 14 TGA/DTG curves of clay-based AAMs having different precursor content at different ages

precursor, in partial or total replacement of GGBS. The following conclusions can be drawn:

- Isothermal calorimetry measurements reveal that a higher amount of solid activator leads to quicker and more intense reaction. However, overdosing of solid activator results in the widespread presence of unreacted or partially hydrated sodium disilicate.
- The incorporation of slag in the precursor blend considerably contributes to a quicker reaction due to the accelerated formation of C–A–S–H.
- All AAMs exhibit workability similar to that of comparable standard cement-based mixes and increasing the amount of solid activator results in higher flowability. On the other hand, the use of slag as a precursor seems to penalize the workability of the blends, even though calcined clay features a distinctively higher water retention capacity.
- The significant shortcomings deriving from the faster setting times of one-part AAMs compared to their cast-in-place cement-based conventional counterparts can be successfully overcome by adjusting the type of precursors, their volume fraction and activator dosage, rather than by increasing the water/binder ratio or using chemical admixtures. In this regard, blends consisting of 81% calcined clay and 19% of slag produced with 22–25% solid activator by weight of the total calcined clay and slag stand out as the most promising candidates.
- The inclusion of a limited amount of slag in clay-based AAM binders is pivotal in refining the pore size distribution and improving the compressive strength of the corresponding mortars, without compromising the fresh properties. Again, blends with 81% calcined clay and 19% of slag offer adequate mechanical response compared to traditional binders.
- An increase in sodium disilicate resulted in higher compressive strength. However, beyond a certain threshold, this increasing rate diminished due to hindered gel coagulation in the presence of excess sodium disilicate.

These results hold the potential to pave the way for the wider use of low-grade calcined clays in one-part AAMs as practical and sustainable alternatives to compete successfully with standard Portland cement, but with dramatically reduced environmental impact for production. It is therefore conceivable that scalable one-part AAM mixtures could be designed by selecting appropriate raw materials based on the local availability of clay resources worldwide.

Acknowledgements The authors thank to Scientific and Technological Research Council of Türkiye (TUBITAK) 2219-Postdoctoral Research Fellowship Program with project number 1059B192100415.

Funding Open Access funding enabled and organized by Projekt DEAL.

Data availability The data supporting the findings of this study are available upon reasonable request.

References

1. Schneider M, Romer M, Tschudin M, Bolio H (2011) Sustainable cement production—present and future. Cem Concr Res 41:642–650. https://doi.org/10.1016/j.cemconres.2011.03.019
2. OECD HIGHLIGHTS Global Material Resources Outlook To 2060–Economic Drivers And Environmental Consequences, 2018.
3. Andrew RM (2018) Global CO_2 emissions from cement production. Earth Syst Sci Data 10:195–217. https://doi.org/10.5194/essd-10-195-2018
4. Gartner E, Hirao H (2015) A review of alternative approaches to the reduction of CO2 emissions associated with the manufacture of the binder phase in concrete. Cem Concr Res 78:126–142. https://doi.org/10.1016/j.cemconres.2015.04.012
5. Provis JL, Palomo A, Shi C (2015) Advances in understanding alkali-activated materials. Cem Concr Res 78:110–125. https://doi.org/10.1016/j.cemconres.2015.04.013

6. Provis JL (2014) Geopolymers and other alkali activated materials: why, how, and what? Mater Struct 47:11–25. https://doi.org/10.1617/s11527-013-0211-5
7. Luukkonen T, Abdollahnejad Z, Yliniemi J et al (2018) One-part alkali-activated materials: a review. Cem Concr Res 103:21–34. https://doi.org/10.1016/j.cemconres.2017.10.001
8. Heath A, Paine K, McManus M (2014) Minimising the global warming potential of clay based geopolymers. J Clean Prod 78:75–83. https://doi.org/10.1016/j.jclepro.2014.04.046
9. Scrivener K, Martirena F, Bishnoi S, Maity S (2018) Calcined clay limestone cements (LC3). Cem Concr Res 114:49–56. https://doi.org/10.1016/j.cemconres.2017.08.017
10. Yang K-H, Song J-K, Song K-I (2013) Assessment of CO2 reduction of alkali-activated concrete. J Clean Prod 39:265–272. https://doi.org/10.1016/j.jclepro.2012.08.001
11. Habert G, Ouellet-Plamondon C (2016) Recent update on the environmental impact of geopolymers. RILEM Tech Lett 1:17–23. https://doi.org/10.21809/rilemtechlett.2016.6
12. Flatt RJ, Roussel N, Cheeseman CR (2012) Concrete: an eco material that needs to be improved. J Eur Ceram Soc 32:2787–2798. https://doi.org/10.1016/j.jeurceramsoc.2011.11.012
13. Duxson P, Mallicoat SW, Lukey GC et al (2007) The effect of alkali and Si/Al ratio on the development of mechanical properties of metakaolin-based geopolymers. Colloids Surf A Physicochem Eng Asp 292:8–20. https://doi.org/10.1016/j.colsurfa.2006.05.044
14. Provis JL (2018) Alkali-activation of calcined clays – past, present and future. In: Martirena F, Favier A, Scrivener K (eds) Calcined clays for sustainable concrete. Springer Netherlands, Dordrecht, pp 372–376
15. Wang L, Zhu Z, Hamza Ahmed A et al (2023) Self-healing behavior of high-strength strain-hardening cement-based composites (HS-SHCC) blended with limestone calcined clay cement (LC3). Constr Build Mater 370:130633. https://doi.org/10.1016/j.conbuildmat.2023.130633
16. Khalifa AZ, Cizer Ö, Pontikes Y et al (2020) Advances in alkali-activation of clay minerals. Cem Concr Res 132:106050. https://doi.org/10.1016/j.cemconres.2020.106050
17. Ferraris G, Christidis GE (2010) Advances in the characterization of industrial minerals. European Mineralogical Union
18. Duxson P, Fernández-Jiménez A, Provis JL et al (2007) Geopolymer technology: the current state of the art. J Mater Sci 42:2917–2933. https://doi.org/10.1007/s10853-006-0637-z
19. Segura IP, Luukkonen T, Yliniemi J et al (2022) Comparison of one-part and two-part alkali-activated metakaolin and blast furnace slag. J Sustain Metall 8:1816–1830. https://doi.org/10.1007/s40831-022-00606-9
20. Khale D, Chaudhary R (2007) Mechanism of geopolymerization and factors influencing its development: a review. J Mater Sci 42:729–746. https://doi.org/10.1007/s10853-006-0401-4
21. Dadsetan S, Siad H, Lachemi M et al (2022) Sodium glass liquid from glass waste as a user-friendly hardener in structural geopolymer systems. Cem Concr Compos 130:104525. https://doi.org/10.1016/j.cemconcomp.2022.104525
22. Duxson P, Provis JL (2008) Designing precursors for geopolymer cements. J Am Ceram Soc 91:3864–3869. https://doi.org/10.1111/j.1551-2916.2008.02787.x
23. Nematollahi B, Sanjayan J, Shaikh FUA (2015) Synthesis of heat and ambient cured one-part geopolymer mixes with different grades of sodium silicate. Ceram Int 41:5696–5704. https://doi.org/10.1016/j.ceramint.2014.12.154
24. Peng MX, Wang ZH, Shen SH et al (2017) Alkali fusion of bentonite to synthesize one-part geopolymeric cements cured at elevated temperature by comparison with two-part ones. Constr Build Mater 130:103–112. https://doi.org/10.1016/j.conbuildmat.2016.11.010
25. Zhang H-Y, Liu J-C, Wu B (2021) Mechanical properties and reaction mechanism of one-part geopolymer mortars. Constr Build Mater 273:121973. https://doi.org/10.1016/j.conbuildmat.2020.121973
26. Choo H, Lim S, Lee W, Lee C (2016) Compressive strength of one-part alkali activated fly ash using red mud as alkali supplier. Constr Build Mater 125:21–28. https://doi.org/10.1016/j.conbuildmat.2016.08.015
27. Ma C, Long G, Shi Y, Xie Y (2018) Preparation of cleaner one-part geopolymer by investigating different types of commercial sodium metasilicate in China. J Clean Prod 201:636–647. https://doi.org/10.1016/j.jclepro.2018.08.060
28. Masi G, Filipponi A, Bignozzi MC (2021) Fly ash-based one-part alkali activated mortars cured at room temperature: effect of precursor pre-treatments. Open Ceram 8:100178. https://doi.org/10.1016/j.oceram.2021.100178
29. Ren J, Sun H, Li Q et al (2021) Experimental comparisons between one-part and normal (two-part) alkali-activated slag binders. Constr Build Mater 309:125177. https://doi.org/10.1016/j.conbuildmat.2021.125177
30. Garg N, White CE (2017) Mechanism of zinc oxide retardation in alkali-activated materials: an in situ X-ray pair distribution function investigation. J Mater Chem A 5:11794–11804. https://doi.org/10.1039/C7TA00412E
31. Partschefeld S, Tutal A, Halmanseder T, Osburg A (2023) Studies on the compatibility of different superplasticizers with alkaline activators for low calcium geopolymer binders. ce papers 6:484–490. https://doi.org/10.1002/cepa.2799
32. Fernández-Jiménez A, Palomo A, Criado M (2005) Microstructure development of alkali-activated fly ash cement: a descriptive model. Cem Concr Res 35:1204–1209. https://doi.org/10.1016/j.cemconres.2004.08.021
33. Ouellet-Plamondon C, Habert G (2015) Life cycle assessment (LCA) of alkali-activated cements and concretes. Handbook of alkali-activated cements, mortars and concretes. Elsevier, pp 663–686
34. Shang J, Dai J-G, Zhao T-J et al (2018) Alternation of traditional cement mortars using fly ash-based geopolymer mortars modified by slag. J Clean Prod 203:746–756. https://doi.org/10.1016/j.jclepro.2018.08.255

35. Wang L, Ur Rehman N, Curosu I et al (2021) On the use of limestone calcined clay cement (LC3) in high-strength strain-hardening cement-based composites (HS-SHCC). Cem Concr Res 144:106421. https://doi.org/10.1016/j.cemconres.2021.106421
36. Peng MX, Wang ZH, Xiao QG et al (2017) Effects of alkali on one-part alkali-activated cement synthesized by calcining bentonite with dolomite and Na_2CO_3. Appl Clay Sci 139:64–71. https://doi.org/10.1016/j.clay.2017.01.020
37. Rovnaník P (2010) Effect of curing temperature on the development of hard structure of metakaolin-based geopolymer. Constr Build Mater 24:1176–1183. https://doi.org/10.1016/j.conbuildmat.2009.12.023
38. Rahman MM, Law DW, Patnaikuni I et al (2021) Low-grade clay as an alkali-activated material. Appl Sci (Basel) 11:1648. https://doi.org/10.3390/app11041648
39. ASTM C807–21 Standard Test Method for Time of Setting of Hydraulic Cement Mortar by Modified Vicat Needle
40. EN 1015–3:2007, Methods of Test for Mortar for Masonry - Part 3: Determination of Consistence of Fresh Mortar (By Flow Table), German Institute for Standardisation (Deutsches Institut für Normung) (2007).
41. Zhou S, Ma C, Long G, Xie Y (2020) A novel non-Portland cementitious material: mechanical properties, durability and characterization. Constr Build Mater 238:117671. https://doi.org/10.1016/j.conbuildmat.2019.117671
42. Sun Z, Vollpracht A (2018) Isothermal calorimetry and in-situ XRD study of the NaOH activated fly ash, metakaolin and slag. Cem Concr Res 103:110–122. https://doi.org/10.1016/j.cemconres.2017.10.004
43. Chithiraputhiran S, Neithalath N (2013) Isothermal reaction kinetics and temperature dependence of alkali activation of slag, fly ash and their blends. Constr Build Mater 45:233–242. https://doi.org/10.1016/j.conbuildmat.2013.03.061
44. Shi C, Roy D, Krivenko P (2003) Alkali-activated cements and concretes, 0 ed. CRC Press
45. Yang K-H, Song J-K (2009) Workability loss and compressive strength development of cementless mortars activated by combination of sodium silicate and sodium hydroxide. J Mater Civ Eng 21:119–127. https://doi.org/10.1061/(ASCE)0899-1561(2009)21:3(119)
46. Gonçalves M, Vilarinho IS, Capela M et al (2021) Waste-based one-part alkali activated materials. Materials (Basel) 14:2911. https://doi.org/10.3390/ma14112911
47. Kim T, Kang C (2021) Investigation of the effect of mixing time on the mechanical properties of alkali-activated cement mixed with fly ash and slag. Materials (Basel) 14:2301. https://doi.org/10.3390/ma14092301
48. Yousefi Oderji S, Chen B, Ahmad MR, Shah SFA (2019) Fresh and hardened properties of one-part fly ash-based geopolymer binders cured at room temperature: effect of slag and alkali activators. J Clean Prod 225:1–10. https://doi.org/10.1016/j.jclepro.2019.03.290
49. Bature AS, Khorami M, Ganjian E, Tyrer M (2021) Influence of alkali activator type and proportion on strength performance of calcined clay geopolymer mortar. Constr Build Mater 267:120446. https://doi.org/10.1016/j.conbuildmat.2020.120446
50. Alhamdan, A. (2018), Shrinkage Behaviour of One and Two Part Alkali-Activated Mortars: Factors and Mitigation Techniques, A Thesis in The Department of Building, Civil and Environmental Engineering, Concordia University, Montréal, Quebec, Canada
51. ASTM C150/C150M (2022) Standard Specification for Portland Cement
52. Ma C, Zhao B, Guo S et al (2019) Properties and characterization of green one-part geopolymer activated by composite activators. J Clean Prod 220:188–199. https://doi.org/10.1016/j.jclepro.2019.02.159
53. Pangdaeng S, Phoo-ngernkham T, Sata V, Chindaprasirt P (2014) Influence of curing conditions on properties of high calcium fly ash geopolymer containing Portland cement as additive. Mater Des 53:269–274. https://doi.org/10.1016/j.matdes.2013.07.018
54. Zhang D-W, Wang D-M, Xie F-Z (2019) Microrheology of fresh geopolymer pastes with different NaOH amounts at room temperature. Constr Build Mater 207:284–290. https://doi.org/10.1016/j.conbuildmat.2019.02.149
55. Elzeadani M, Bompa DV, Elghazouli AY (2022) One part alkali activated materials: a state-of-the-art review. J Build Eng 57:104871. https://doi.org/10.1016/j.jobe.2022.104871
56. Ismail I, Bernal SA, Provis JL et al (2014) Modification of phase evolution in alkali-activated blast furnace slag by the incorporation of fly ash. Cem Concr Compos 45:125–135. https://doi.org/10.1016/j.cemconcomp.2013.09.006
57. Yip CK, Lukey GC, Van Deventer JSJ (2005) The coexistence of geopolymeric gel and calcium silicate hydrate at the early stage of alkaline activation. Cem Concr Res 35:1688–1697. https://doi.org/10.1016/j.cemconres.2004.10.042
58. Deir E, Gebregziabiher BS, Peethamparan S (2014) Influence of starting material on the early age hydration kinetics, microstructure and composition of binding gel in alkali activated binder systems. Cem Concr Compos 48:108–117. https://doi.org/10.1016/j.cemconcomp.2013.11.010
59. van Jaarsveld, J. G. S. (2000). The physical and chemical characterisation of fly ash based geopolymers. PhD thesis, Department of Chemical Engineering, The University of Melbourne.
60. Zeng Q, Li K, Fen-Chong T, Dangla P (2016) Pore structure of cement pastes through NAD and MIP analysis. Adv Cem Res 28:23–32. https://doi.org/10.1680/adcr.14.00109
61. Ali Shah SF, Chen B, Ahmad MR, Haque MA (2021) Development of cleaner one-part geopolymer from lithium slag. J Clean Prod 291:125241. https://doi.org/10.1016/j.jclepro.2020.125241
62. Li J, Mailhiot S, Sreenivasan H et al (2021) Curing process and pore structure of metakaolin-based geopolymers: liquid-state 1H NMR investigation. Cem Concr Res 143:106394. https://doi.org/10.1016/j.cemconres.2021.106394
63. Zhang Y, He Y, Cui X, Liu L (2023) Enhancing freeze-thaw resistance of alkali-activated slag by metakaolin. ACS Omega 8:20869–20880. https://doi.org/10.1021/acsomega.3c01600
64. Shi C, Qu B, Provis JL (2019) Recent progress in low-carbon binders. Cem Concr Res 122:227–250. https://doi.org/10.1016/j.cemconres.2019.05.009
65. Rivera OG, Long WR, Weiss CA Jr et al (2016) Effect of elevated temperature on alkali-activated geopolymeric binders compared to portland cement-based binders. Cem Concr Res 90:43–51. https://doi.org/10.1016/j.cemconres.2016.09.013

66. Tu W, Zhang M (2023) Behaviour of alkali-activated concrete at elevated temperatures: a critical review. Cem Concr Compos 138:104961. https://doi.org/10.1016/j.cemconcomp.2023.104961